Self-assembled Ag(111) nanostructures induced by Fermi surface nesting

Timothy E. Kidd ⬤, Evan O'Leary, Aaron Anderson, Skylar Scott, and Andrew J. Stollenwerk
Physics Department, University of Northern Iowa, Cedar Falls, Iowa 50614, USA

Scanning tunneling microscopy measurements on Ag(111)/MoS$_2$ reveal atomically flat preferred, or "magic," heights occurring at 6, 10, and 14 atomic layers. These results are consistent with Ag growth on a variety of semiconducting substrates and correlate with electronic energy savings in electronic structure calculations of freestanding Ag(111) films. Thus, under certain conditions, Ag will spontaneously form quantized structures independent of the substrate. To explain this, we have found Fermi surface nesting vectors in the bulk Ag band structure which account for these results and the fact Ag that is gapped along the surface normal. This model extends to a range of metallic systems which exhibit electronic confinement, epitaxial growth, and minimal strain. As with Au/MoS$_2$, the Ag/MoS$_2$ system exhibits this behavior at unusually high temperatures so that these principles might be used for control over device features at the nanometer scale under standard fabrication conditions.

I. INTRODUCTION

Under certain conditions, thin metallic films will self-assemble into specific structures according to their electronic properties [1]. From electron confinement, quantum well states are formed in the film. The relationship between the location of these states and film thickness results in energy contributions that oscillate with film thickness. The total energy is reduced when the highest occupied quantum well state is farther below the Fermi level (E_F). Thus, preferred or "magic" thicknesses occur periodically at dimensions that minimize the density of states (DOS) near E_F. Self-assembly processes provide the ability to control the dimensions of numerous crystal structures on the nanometer scale with many practical applications such as catalysts [2,3], solar cells [4], or sensor applications [5,6]. In particular, Ag nanocrystals are known to be toxic to a wide variety of microbes and parasites [7]. Unfortunately, self-assembly driven by quantum well states is hindered by a number of constraints.

Typically, these quantum size effects are dwarfed by classical contributions such as surface kinetics, strain due to lattice mismatch, and surface free energy. Classical contributions can be minimized to observe quantum size effects by using a substrate with a high degree of lattice matching [8] or through the formation of a wetting layer [9] while maintaining precise control over the deposition and subsequent annealing temperatures. Cryogenic growth temperatures are usually required to limit diffusion of the deposited adatoms to allow formation of quantized structures representing local minima in the total energy of the system. The system is "annealed" at or near room temperature for limited surface diffusion to perfect the quantized structure. Materials that meet these criteria and still maintain strong confinement are limited, but preferred heights due to quantum size effects have been observed in several systems, with prototypical cases being Pb/Si(111) [10–12] and Pb/Cu(111) [13].

Recently, we discovered that quantum size effects influence the growth of Au(111) on MoS$_2$ [14]. In this system, quantum size effects are observed in all three dimensions and are observed up to 725 K. The Fermi surface of Au is gapped in the [111] direction, suppressing the formation of standing waves with zero in-plane momentum. Instead, the dimensions correlate with the necks of the Fermi surface along the ⟨111⟩ directions. Perhaps most importantly, this discovery suggests that van der Waals bonding may serve as an alternative mechanism to reduce classical energy contributions and observe quantum size effects in a wide variety of metals.

Ag is a logical choice to contrast with these results since it also grows with a (111) orientation on MoS$_2$ and has an electronic structure similar to Au. Additionally, quantum size effects have already been reported in Ag(111) thin films on a multiple substrates, providing a basis for comparison. Many reports show that Ag islands do not grow with a single atomic layer height above the wetting layer on Si(111). Although the bulk Ag Fermi surface is gapped in the [111] direction, a case is made that interface effects result in expanded lattice constants that close this gap. When an island is only a couple of atomic layers thick, the lattice constant approaches the bulk value and the gap quickly opens again [15–18]. This explanation does not account for the 1.4 nm preferred height in Ag(111) grown on GaAs(110) [19], Ge(111) [20], Si(111) [21], and MoS$_2$(0001) [22]. Nor would it explain the additional preferred height of approximately 2.4 nm seen on Ge and MoS$_2$. Although it has been suggested that the increased stability of these heights is due to quantum size effects, a link between the electronic structure of Ag and these heights has not been established.

II. METHODS

In this paper, we have used scanning tunneling microscopy (STM) to study the surface morphology of Ag(111) grown on MoS$_2$ as a function of coverage and annealing temperature. Our measurements indicate that Ag islands have preferred heights of 1.38 ± 0.05 nm and 2.29 ± 0.09 nm, corresponding

to 6 and 10 atomic layers, respectively. These results agree with those found in literature for Ag(111) islands grown on several different substrates, suggesting these effects are due to the properties of Ag. Furthermore, we also present evidence for an additional stable height at 3.32 ± 0.16 nm or 14 atomic layers. These preferred heights have a four-atomic-layer periodicity that strongly correlates with a particular set of nesting vectors on the Fermi surface of Ag. This periodicity is further confirmed by examining the calculated DOS of freestanding Ag slabs.

Samples were prepared by depositing Ag onto the cleaved surface of commercially available MoS_2 in a vacuum chamber with a base pressure of 9×10^{-11} mbar. Deposition occurred at room temperature using a 2 mm Ag wire (99.999% pure) in a miniature electron-beam evaporator (MANTIS QUAD-EV). A flux monitor was used to maintain a consistent deposition rate calculated to be approximately 0.1 Å/s from the resulting scanning tunneling microscopy images. The error in determining nominal coverage from the STM images is estimated to be $\pm 10\%$. Ag was deposited at coverages ranging from approximately 0.5 to 4.0 nm. These samples were annealed using resistive heating and temperature was monitored using a type K thermocouple in contact with the preparation stage. Heating was performed at temperature for at least 10 minutes. This time was found to be sufficient for the surface to reach equilibrium by comparing surfaces annealed up to 12 hours. Prepared samples were transferred *in situ* to the adjacent variable temperature STM head (Omicron). STM tips were electrochemically etched from a 0.25 mm W wire in a 5 M potassium hydroxide solution with a 5 V DC bias or mechanically cut from a 0.25 mm $Pt_{90}Ir_{10}$ wire. Scanning parameters used in this study were relatively consistent. The tunneling bias typically ranged from 0.75 to 1.5 V and the current set point varied from 0.5 to 5 nA. No significant differences were observed between extremal scanning parameters.

Density functional theory (DFT) was used to calculate the DOS of Ag(111). The crystal structure and lattice constants used in this calculation were derived from experimental results [23]. An additional 1.5 nm vacuum spacing was added to the unit cell in the z direction to avoid wave function overlap. The Perdew-Burke-Ernzerhof implementation [24] of the generalized gradient approximation (PBE GGA) was used within the ATOMISTIX TOOLKIT package [25–27]. Convergence with respect to the k-point mesh was relatively slow, requiring a mesh of $70 \times 70 \times 1$.

III. RESULTS AND DISCUSSION

Cross sections from all images taken of Ag films reveal that the Ag forms atomically flat, plateaued islands that were stable for several weeks at base pressure. The atomic step height of the Ag in these images is consistent with past work indicating (111) growth on MoS_2 [28,29]. The Ag islands on all samples had a remarkably uniform distribution of heights (FWHM typically less than 1.0 nm). These properties held true regardless of coverage or annealing temperature.

Surfaces with coverage less than 2.5 nm consisted of small islands with faceted shapes reflecting the symmetry of the MoS_2 substrate. These structures are exemplified by the image from a 0.7 nm thick Ag film depicted in Fig. 1(a). The
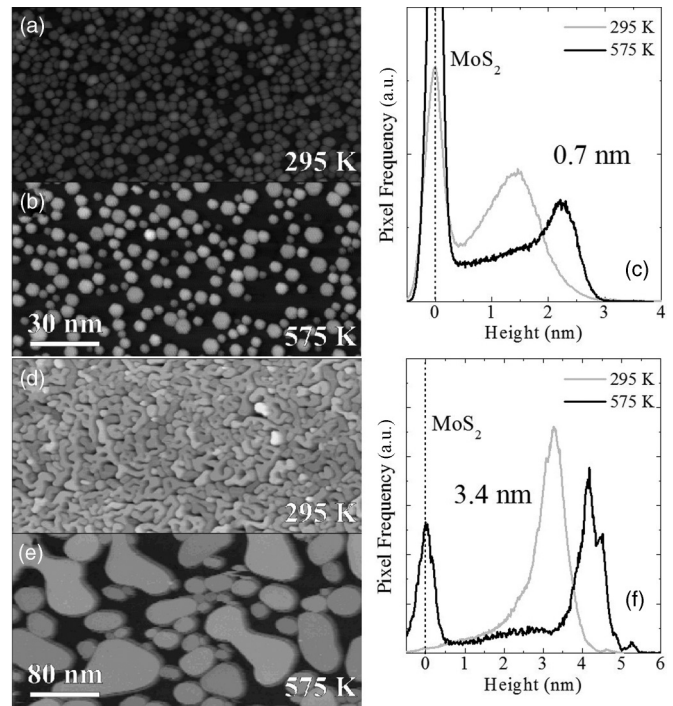

FIG. 1. STM images of Ag(111) islands on MoS_2 with a 0.7 nm nominal coverage (a) before and (b) after annealing. The height distributions calculated from these images are shown in (c). A dashed line indicates the location of the MoS_2 substrate. STM images of the same system with a 3.4 nm coverage (d) before and (e) after annealing. The height distributions calculated from these images are shown in (f). Panels (a) and (b) shares the same scale bar, as do panels (c) and (d).

image in Fig. 1(b) shows this same surface after annealing to 575 K. The average lateral dimensions have clearly increased and nearly every island has assumed the shape of a regular hexagon. The preferred height of the Ag islands has also increased from about 1.40 to 2.25 nm as demonstrated by the height distributions plotted in Fig. 1(c). The estimated error in determining the preferred heights is ± 0.24 nm, or one atomic layer of Ag(111).

Following room temperature deposition, films with coverages greater than 2.5 nm were composed of irregular, elongated structures with no obvious correlation to the MoS_2 substrate. The image of a 3.4 nm thick film in Fig. 1(d) shows that these structures are not continuous but do cover nearly the entire substrate. In most cases, the absolute height of films thicker than 2.5 nm could not be determined before annealing because the substrate was not visible. After annealing to 575 K [Fig. 1(e)], a significantly larger portion of the MoS_2 is visible. The nearly continuous structures have transformed into a mixture of irregular and facetted islands. The preferred height of the Ag islands increased from about 3.25 to 4.15 nm when annealed as shown in Fig. 1(f). Two peaks can be seen in Fig. 1(f). Their height difference corresponds to a single atomic Au(111) layer. A single atom step height was not unusual to find on the flat plateaus for this sample, indicating both heights have similar stability. The broad feature hump seen between 2 and 3 nm of Fig. 1(f) could be an artifact
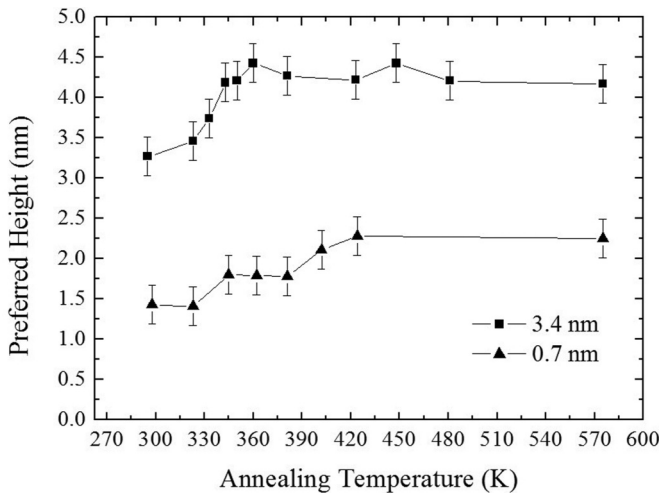
FIG. 2. Preferred height of Ag(111) islands on MoS_2 as a function of annealing temperature for 0.7 and 3.4 nm coverages.

FIG. 3. STM images of annealed Ag(111) islands on MoS_2 and corresponding height distributions for nominal coverages of (a) 0.46, (b) 0.99, and (c) 1.57 nm. A dashed line indicates the location of the MoS_2 substrate. All images are 150 nm×150 nm.

arising from an imperfect STM tip. Such artifacts can arise at intermediate heights in an STM image, which is why only the tallest features were included in the actual analysis.

The plot in Fig. 2 shows the shift in preferred island height of the 0.7 and 3.4 nm thick samples as a function of annealing temperature. In both cases, the preferred island height quickly increases before reaching an equilibrium state between approximately 350 and 425 K, and definitely established by 500 K. Figure 3 shows images and corresponding height distributions of fully annealed 0.46, 0.99, and 1.57 nm thick Ag films. The islands increase in lateral size with additional material. In contrast, the height distributions show the most probable island height stays consistent at about 2.25 nm, even as the amount of Ag is tripled. In a different study, a similar preferred height was observed on an annealed 0.3 nm thick Ag film on MoS_2 [22].

The coverage dependence is explored further in Fig. 4(a). The preferred height of 2.25 nm is stable up to coverages of 2.0 nm. At increased up to 3.0 nm, the next stable preferred height is at 3.3 nm. Above this, the preferred height is no longer stable, increasing with coverage. Unannealed preferred island heights are included in Fig. 4(a) (grey triangles). Two of these preferred heights, at 2.25 and 3.3 nm, correspond to the stable features measured on the annealed samples. There is also an additional stable preferred height at 1.4 nm, which was only found before annealing. This same stable height was observed in another study in unannealed Ag films on MoS_2 down to a third of an atomic layer [22]. This height would appear to be metastable as it is not present at elevated temperatures.

In Fig. 4(a), dashed lines are used to indicate the average value of the stable heights calculated to be 1.38 ± 0.05 nm, 2.29 ± 0.09 nm, and 3.32 ± 0.16 nm corresponding to 6, 10, and 14 atomic layers, respectively. The average spacing of these stable heights is 0.97 nm, roughly four atomic layers. As seen in Fig. 4(b), the DFT calculations show periodic dips in the DOS of Ag(111) at E_F with an interval of 1.2 nm or five atomic layers. The periodicity of these stable energy configurations is in good agreement with our experimental
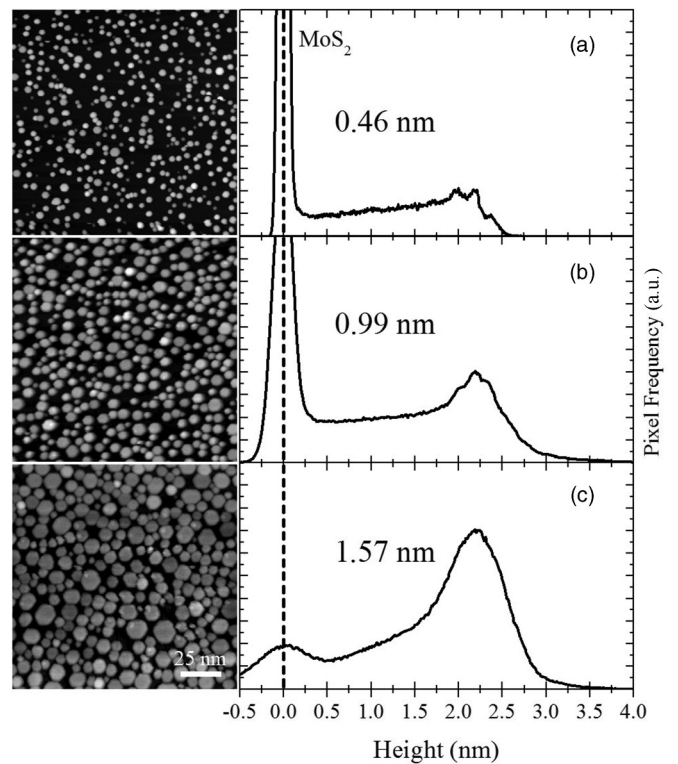
results. These calculations were carried out on freestanding slabs of Ag(111), suggesting minimal influence from the MoS_2. We conclude our results are largely due to the electronic structure of Ag. Results found in literature support this conclusion. Specifically, the first two stable heights presented here have been observed in Ag(111) films grown on four different substrates [19–22].

The results indicate the physical and electronic structure are strongly coupled in ultrathin Ag(111) films. Confinement effects arising from quantization of perpendicular momentum influence the number states at E_F and film stability. In the simplest model, only electrons with zero parallel momentum are considered when calculating quantum well states. This does not hold here as there are no states at the Fermi level in the [111] direction of Ag. However, perpendicular momentum can be quantized even if there is a nonzero parallel component. Systems with Fermi surface topologies that have parallel faces spanned by a nesting vector, **q**, are of particular interest [30]. Introducing a periodicity associated with a nesting vector opens a gap in the DOS along the entire parallel face, disproportionally decreasing the electronic energy of the system. This is similar to the relationship between nesting vectors and the tendency toward charge density wave order in certain materials [31]. Assuming conservation of parallel momentum, only nesting vectors normal to the surface are considered. Contributions to the DOS at E_F are at a maximum when the island height, given as a discrete number of layers (N) with interlayer distance (d), are an integer multiple
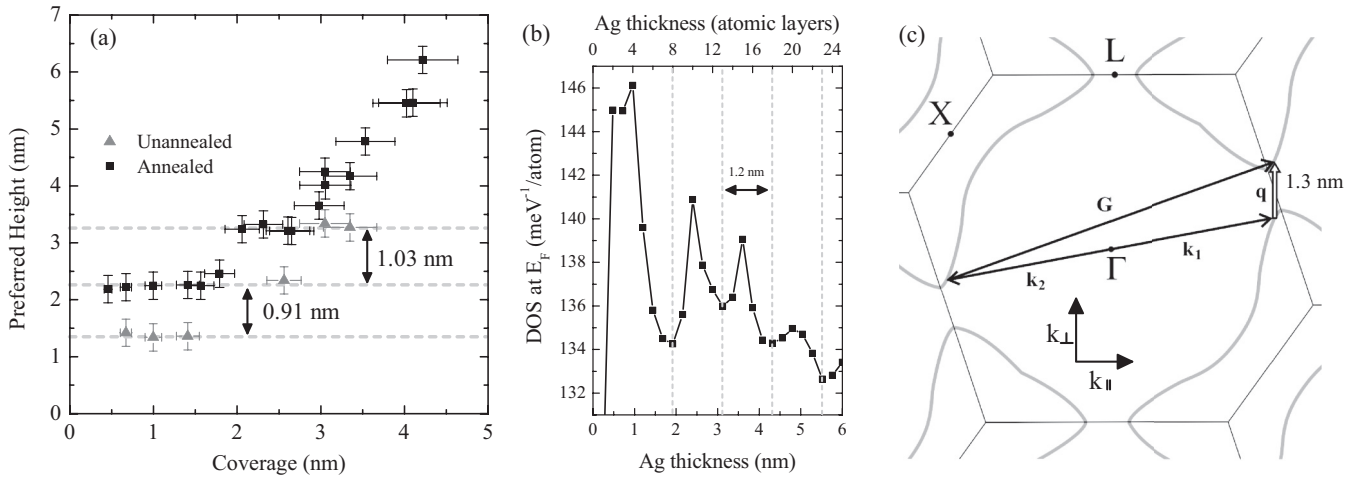
FIG. 4. (a) Preferred island heights as a function of nominal Ag coverage on MoS_2 for unannealed (solid grey triangles) and annealed surfaces (solid black squares). Horizontal, dashed grey lines mark island heights exhibiting increased stability. The average spacing between stable heights is 0.97 nm or about four atomic layers. (b) Calculated DOS of freestanding Ag(111) slabs at the Fermi level as a function of Ag thickness. The spacing between local minima in the DOS is 1.2 nm or five atomic layers. (c) Cross section of the Fermi surface of Ag in the [111] direction perpendicular to the substrate. The nesting vector is labeled as **q** and spans the vectors **k_1** and **k_2** after translation back to the first Brillouin zone. From Eq. (1), the periodicity associated with this vector is 1.3 nm.

of $2\pi/q$,

$$Nd = n\frac{2\pi}{q}. \qquad (1)$$

In Fig. 4(c) we examine the bulk Ag Fermi surface cut along the [111] direction (adapted from Ref. [32]). The nesting vector labeled here crosses into the second Brillouin zone and can be represented as spanning two points on the Fermi surface by momentum vectors **k_1** and **k_2** translated back into the first Brillouin zone by the reciprocal lattice vector, **q** = **k_1**−(**k_2** + **G**). The corresponding periodicity of stable heights expected from this nesting vector is estimated to be approximately 1.3 nm according to Eq. (1), within approximately one atomic layer of the experimental and computational results.

IV. CONCLUSIONS

We have shown that Ag(111) islands grown on MoS_2 spontaneously form preferred heights of increased stability depending on coverage and temperature. The periodic spacing of these heights is four atomic layers, consistent with dips in the DOS at the Fermi level of freestanding Ag(111) slabs calculated using DFT. The periodic reduction in the DOS and the resulting stable heights arise from Fermi surface nesting vectors along the Ag(111) surface normal direction that

incorporate the Ag reciprocal lattice vector. Preferred heights with intervals associated with this nesting have lower overall energy from the formation of gaps over the relevant portions of the Fermi surface. In addition to providing a substrate independent model for quantized metallic film growth, this work identifies an influential nesting vector that could strengthen theories that govern long-range ferromagnetism [33,34]. Ag, along with Au, grown on MoS_2 represent a new class of self-assembled growth in which structural quantization arises from quantum confinement at unusually high temperatures suitable for standard device fabrication. There are many such metal–van der Waals systems which exhibit epitaxial growth [35,36] and show excellent potential for extending this work beyond noble metals to explore superconducting or magnetic phases as well.

[1] Z. Zhang, Q. Niu, and C. K. Shih, Phys. Rev. Lett. **80**, 5381 (1998).

[2] J. Chen, B. Lim, E. P. Lee, and Y. Xia, Nano Today **4**, 81 (2009).

[3] H. Zhang, M. Jin, Y. Xiong, B. Lim, and Y. Xia, Acc. Chem. Res. **46**, 1783 (2013).

[4] M. Yuan, M. Liu, and E. H. Sargent, Nat. Energy **1**, 16016 (2016).

[5] M. Epifani, E. Comini, R. Díaz, A. Genç, T. Andreu, P. Siciliano, and J. R. Morante, J. Alloys Compd. **665**, 345 (2016).

[6] M. Sriram, K. Zong, R. S. Vivekchand, and J. J. Gooding, Sensors **15**, 25774 (2015).

[7] B. Le Ouay and F. Stellacci, Nano Today **10**, 339 (2015).

[8] K. L. Man, Z. Q. Qiu, and M. S. Altman, Phys. Rev. B **81**, 045426 (2010).

[9] M. Miyazaki and H. Hirayama, Surf. Sci. **602**, 276 (2008).

[10] V. Yeh, L. Berbil-Bautista, C. Z. Wang, K. M. Ho, and M. C. Tringides, Phys. Rev. Lett. **85**, 5158 (2000).

[11] W. B. Su, S. H. Chang, W. B. Jian, C. S. Chang, L. J. Chen, and T. T. Tsong, Phys. Rev. Lett. **86**, 5116 (2001).

[12] R. Otero, A. L. Vázquez de Parga, and R. Miranda, Phys. Rev. B **66**, 115401 (2002).

[13] B. J. Hinch, C. Koziol, J. P. Toennies, and G. Zhang, Europhys. Lett. **10**, 341 (1989).

[14] T. E. Kidd, J. Weber, R. Holzapfel, K. Doore, and A. J. Stollenwerk, Appl. Phys. Lett. **113**, 191603 (2018).

[15] Y. Chen, M. W. Gramlich, S. T. Hayden, and P. F. Miceli, Phys. Rev. Lett. **114**, 035501 (2015).

[16] B. Ünal, A. Belianinov, P. A. Thiel, and M. C. Tringides, Phys. Rev. B **81**, 085411 (2010).

[17] L. Gavioli, K. R. Kimberlin, M. C. Tringides, J. F. Wendelken, and Z. Zhang, Phys. Rev. Lett. **82**, 129 (1999).

[18] P. Sobotík, I. Ošt'ádal, J. Mysliveček, T. Jarolímek, and F. Lavický, Surf. Sci. **482–485**, 797 (2001).

[19] A. R. Smith, K. J. Chao, Q. Niu, and C. K. Shih, Science **273**, 226 (1996).

[20] F. Krok, F. Buatier de Mongeot, M. Goryl, J. J. Kolodziej, and M. Szymonski, Phys. Rev. B **81**, 235414 (2010).

[21] L. Huang, S. Jay Chey, and J. H. Weaver, Surf. Sci. **416**, L1101 (1998).

[22] C.-H.-T. Chang, H.-H. Chang, P.-C. Jiang, and W.-B. Su, Jpn. J. Appl. Phys. **57**, 08NB10 (2018).

[23] J. Rumble, *CRC Handbook of Chemistry and Physics* (CRC Press, Boca Raton, FL, 2017).

[24] J. P. Perdew, K. Burke, and M. Ernzerhof, Phys. Rev. Lett. **77**, 3865 (1996).

[25] Atomistix toolkit version 13.8.1, www.quantumwise.com.

[26] M. Brandbyge, J.-L. Mozos, P. Ordejón, J. Taylor, and K. Stokbro, Phys. Rev. B **65**, 165401 (2002).

[27] J. M. Soler, E. Artacho, J. D. Gale, A. García, J. Junquera, P. Ordejón, and D. Sánchez-Portal, J. Phys.: Condens. Matter **14**, 2745 (2002).

[28] C. Gong, C Huang, J. Miller, L. Cheng, Y. Hao, D. Cobden, J. Kim, R. S. Ruoff, R. M. Wallace, K. Cho, X. Xu, and Y. J. Chabal, ACS Nano **7**, 11350 (2013).

[29] S. Mahatha and K. S. Menon, J. Phys.: Condens. Matter **24**, 305502 (2012).

[30] M. D. Stiles, Phys. Rev. B **48**, 7238 (1993).

[31] M. H. Whangbo, E. Canadell, P. Foury, and J. P. Pouget, Science **252**, 96 (1991).

[32] N. Ashcroft and D. Mermin, *Solid State Physics* (Thomson Learning, Stamford, CT, 1976).

[33] F. Herman and R. Schrieffer, Phys. Rev. B **46**, 5806 (1992).

[34] E. Mendive-Tapia and J. B. Staunton, Phys. Rev. Lett. **118**, 197202 (2017).

[35] A. C. Domask, K. A. Cooley, B. Kabius, M. Abraham, and S. E. Mohney, Cryst. Growth Des. **18**, 3494 (2018).

[36] K. A. Cooley, R. Alsaadi, R. L. Gurunathan, A. C. Domask, L. Kerstetter, W. A. Saidi, and S. E. Mohney, J. Cryst. Growth **505**, 44 (2019).